Journal of Materials Chemistry A

Accepted Manuscript

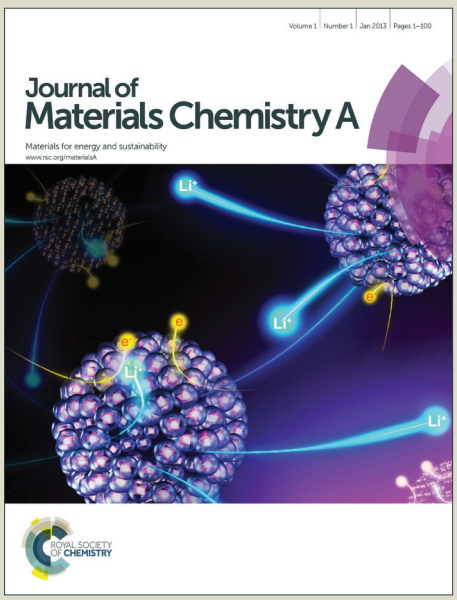

ROYAL SOCIETY OF CHEMISTRY

www.rsc.org/materialsA

Journal Name

ARTICLE

Niobium doped anatase TiO_2 as an effective anode material for sodium-ion batteries

Received 00th January 20xx,
Accepted 00th January 20xx

DOI: 10.1039/x0xx00000x

www.rsc.org/

Fei Zhao[a], Baofeng Wang[a,b,*], Yufeng Tang[c], Zhenguo Huang[b,*], Honghua Ge[a] ,Hua Kun Liu[b]

Sodium-ion batteries are considered to be a promising low-cost alternative to common lithium-ion batteries in the areas where specific energy is less critical. Among all the anode materials studied so far, TiO_2 is very promsing due to its low operation voltage, high capacity, nontoxicity, and low production cost. Herein, we present Nb-doped anatase TiO_2 nanoparticles with high capacity, excellent cycling performance, and excellent rate capability. The optimized Nb-doped TiO_2 anode delivers a high reversible capacity of 177 mAh/g at 0.1 C and 108.8 mAh/g at 5 C, in contrast to 150.4 mAh/g at 0.1 C and only 54.6 mAh/g at 5 C for the pristine TiO_2. The good performance is likely to be associated with enhanced conductivity and lattice expansion due to Nb doping. These results, in combination with its environmental friendliness and cost efficiency, render Nb-doped TiO_2 a promising anode material for high-power sodium-ion batteries.

Introduction

Rechargeable batteries play an important role in powering portable electronic devices and in grid-level electricity storage for green energy systems such as wind and solar[1-4]. Although lithium-ion batteries (LIBs) represent the state-of-the-art technology in high-energy storage, there are still challenges facing this technology such as limited Li sources and cost[5, 6]. To address these issues, rechargeable sodium-ion batteries (NIBs) are proposed as a potential candidate for large-scale energy storage due to the natural abundance and lower cost of sodium [7, 8]. For the NIB anode materials, much effort has been focused on low-voltage metal oxide anodes, among which, TiO_2 has attracted considerable attention[2, 9-13] due to its low operation voltage, high capacity, nontoxicity, and low production cost.

Recently, various polymorphs of TiO_2, such as rutile[14], TiO_2(B)[15] and anatase[9, 16-18] have been studied as anode materials for Na-ion batteries. Among these, three-dimensional Na^+ diffusion is kinetically restricted in micrometer-sized rutile TiO_2, resulting in poor anode performance[14]. TiO_2(B) has low electronic conductivity and a low diffusion coefficient[19]. In comparison, anatase TiO_2 can supply effective diffusion paths and more accommodation sites for Na ions[20]. The conductivity of TiO_2, however, was poor, and its narrow ionic channels are not suitable for rapid sodium ion transportation, leading to low specific capacity and significant capacity loss at high charge-discharge current densities[11, 21]. Doping with aliovalent ions is a facile way to improve the electrical conductivity of TiO_2[22-25]. Very recently, Nb-doped rutile TiO_2 was reported by Usui et al. as anode for NIBs[14]. It was suggested that Nb doping could improve the Na-ion storage performance due to the enhanced conductivity and broadened ionic channels. Those effects are also expected for the Nb-doped anatase TiO_2 anode for NIBs, which has never been investigated.

In this paper, Nb-doped anatase TiO_2 nanoparticles were synthesized by a facile sol-gel method. When used as an anode material for NIBs, they deliverer a high capacity and excellent rate capacity, and this improvement can be ascribed to the widened Na-ion migration channels and much reduced charge-transfer resistance. These advantages make Nb doped TiO_2 a promising anode material for high performance sodium-ion batteries.

Experimental

Preparation of pristine and Nb doped TiO_2 nanoparticles

A series of pristine and Nb doped TiO_2 samples were synthesized by a sol–gel method (shown in Fig. 1). An aqueous solution of $TiO(NO_3)_2$ was first obtained by reacting nitric acid with titanyl hydroxide [TiO-$(OH)_2$], which was obtained by the hydrolysis of tetrabutyl titanate (TBT). The $TiO(NO_3)_2$ (0.02 mol), 8.4 g citric acid (CA), and a certain amount of $NbCl_5$ (atomic ratios of Nb/Ti = 0%, 1%, 2%, 5%） were mixed together. The resulting solution was adjusted to a neutral pH value by adding aqueous ammonia. The mixture was magnetically stirred at 90˚C until a clear viscous gel was

[a] Shanghai Key Laboratory of Materials Protection and Advanced Materials in Electric Power, College of Environmental and Chemical Engineering, Shanghai University of Electric Power, Shanghai 200090, China. Email：wangbaofeng@shiep.edu.cn
[b] Institute for Superconducting & Electronic Materials, University of Wollongong, NSW 2500, Australia
[c] Chinese Academy of Sciences (CAS) Key Laboratory of Materials for Energy Conversion, Shanghai Institute of Ceramics, CAS, Shanghai 200050, China

† Footnotes relating to the title and/or authors should appear here.
Electronic Supplementary Information (ESI) available: [details of any supplementary information available should be included here]. See DOI: 10.1039/x0xx00000x

obtained and then completely dried in an oven at 250˚C for 3 h. Combustion took place in the oven and generated the corresponding oxide product, with CO_2, NO_x, and H_2O as by-products. Finally, the froth-like powders were ground and calcined at 500˚C for 6 h in air to produce Nb doped anatase TiO_2 nanoparticles.

Physical characterization

X-ray diffractometry (XRD, Rigaku RINT 2200) was employed to check the phase of the powder samples. XRD data were obtained with Cu Kα1 radiation (λ = 0.15406 nm) in the 2θ range of 20–60° with a step size of 0.02° and a scan rate of 2° per minute. X-ray photoelectron spectroscopy (XPS) measurements were carried out on a Kratos Axis UltraDLD spectrometer (Kratos Analytical - A Shimadzu Group company) using monochromatic Al Kα radiation (hv =1486.6 eV). The particle shape and morphology of TiO_2 were observed with a scanning electron microscope (SEM, Hitachi S-3500N). Energy dispersive X-ray spectroscopy (EDS, Oxford INCA) was employed to analyse the composition and distribution of elements.

Electrochemical tests

Electrochemical experiments were carried out via CR2016 coin-type test cells assembled in an argon-filled glove box using sodium metal as counter electrode. The composite electrode was made up of the active materials powder (80 wt %), acetylene black (10 wt %), and 10 wt % sodium carboxymethyl cellulose (CMC, WALOCEL™ CRT 2000 PPA 12, Dow Wolff Cellulosics), all of which were mixed together into a slurry and then coated uniformly on copper foil. 1.54 cm^2 disks were punched out of the foil, and the weight of the active material on each disk was about 4.0 mg. The electrolyte was 1 M $NaClO_4$ (98% Sigma Aldrich) in ethylene carbonate (EC) and diethyl carbonate (DEC) (1:1 by volume). The discharge-charge measurements were performed on a Land CT2001A battery tester (Wuhan, China) in constant current mode in the range of 0-2.5 V. The electrochemical impedance spectroscopy (EIS) analysis was performed on an Autolab PGSTAT 302N electrochemical workstation in the frequency range of 100 kHz - 0.1 Hz with potentiostatic signal amplitude of 5 mV. The electrode was activated by one cycle of charge/discharge at 0.1 C (1 C = 330 mAh/g) between 0 V and 2.5 V vs. Na/Na^+ and then discharged to 0.3 V. The EIS test was performed at a stable open circuit voltage after a 6-hour rest of the discharged electrode.

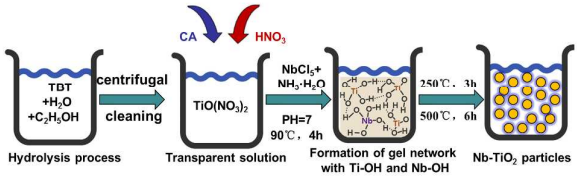

Fig. 1 Synthetic procedure for Nb doped TiO_2. The method is the same for pristine TiO_2, but without the addition of Nb.

Results and Discussion

The XRD patterns of pristine and Nb-doped TiO_2 samples prepared by the sol–gel method and annealed at 500 °C are presented in Fig. 2. All the peaks are in accordance with the standard diffraction peaks of anatase phase TiO_2 (JCPDS No. 21-1272), which indicates that the Nb has been successfully incorporated into the crystal structure of TiO_2. Rietveld refinement of the XRD data reveals a minor increase in the a lattice parameter (shown in Fig. 3), as evidenced by the slight peak shift of the (200) reflection towards lower angles. This noticeable increase in the a parameter has been reported in the literature[26, 27], where the doping level was higher (10 % vs. 5 % in this study). Nb doping has expanded the unit cell, as can be seen from Fig. 3, although the c parameter varies slightly. These are similar to the results reported by Furubayashi et al.[26]. It is well known that the ionic radius of Nb^{5+} (0.64 Å) is slightly larger than that of Ti^{4+} (0.605 Å)[28], and thus, incorporating Nb^{5+} into the TiO_2 framework would slightly expand the lattice of TiO_2. The peak broadening with increasing Nb content indicates smaller crystallite size. By applying the Scherrer equation to the (101) peaks, the average crystallite size of TiO_2 and Nb-TiO_2 are estimated to be 16.07, 12.34, 12.03, 10.17 nm for TiO_2 with 0%, 1%, 2%, 5% Nb, respectively, which is in agreement with a previous report[29].

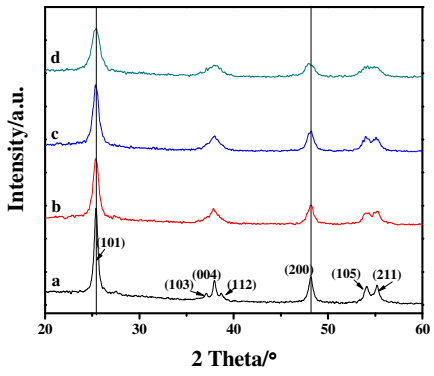

Fig. 2. Powder X-ray diffraction patterns of (a) pristine TiO_2, (b) 1% Nb-doped TiO_2, (c) 2% Nb-doped TiO_2, (d) 5% Nb-doped TiO_2

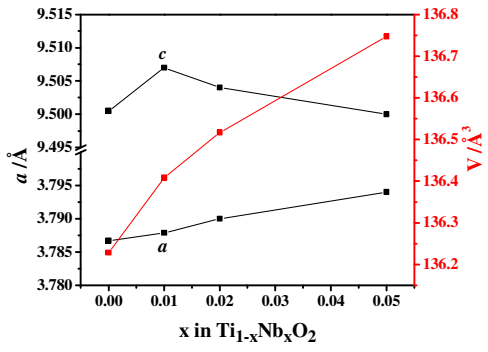

Fig.3. Lattice parameters a, c and cell volume as a function of the doping level in $Ti_{1-x}Nb_xO_2$

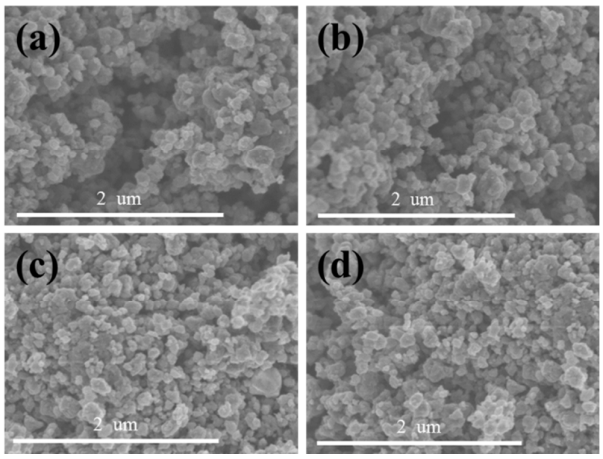

Fig. 4. SEM images of (a) pristine, (b) 1%, (c) 2%, and (d) 5% Nb-doped TiO_2.

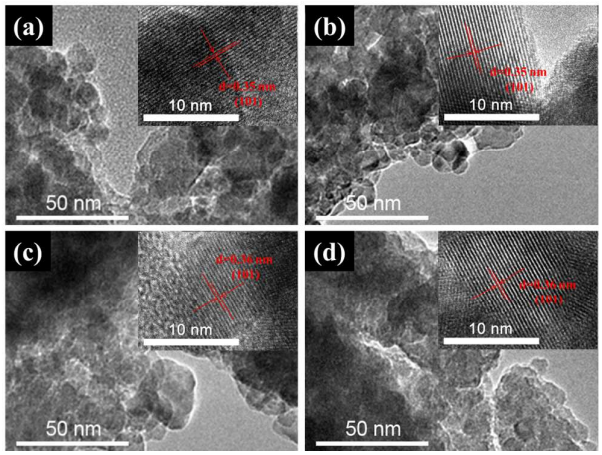

Fig. 5. TEM images of different samples: (a) pristine TiO_2; (b) 1% Nb-doped TiO_2; (c) 2% Nb-TiO_2; and (d) 5% Nb-TiO_2 (insets are high resolution TEM (HRTEM) images).

The SEM images show that all the samples possess a similar morphology, with all four samples consisting of small particles with diameters of 100-300 nm (Fig. 4). The EDS mapping patterns clearly indicate that the Nb is uniformly dispersed in the TiO_2 sample (not shown here).

TEM is used to investigate the microstructure of materials in more detail. Fig. 5a-d presents TEM images of TiO_2 and Nb doped TiO_2, respectively. The pristine and Nb doped TiO_2 particles have a similar particle size (~30 nm in diameter) and morphology. The high-resolution images (insets in Fig. 5) reveal lattice fringes corresponding to the (101) planes, with a slight increase in lattice spacing from 0.35 to 0.36 nm as the doping level of the anatase TiO_2 increases from 0% to 5%. The slight increase in the fringe spacing of TiO_2 indicates that Nb has successfully entered into the lattice of anatase TiO_2, which matches the XRD results.

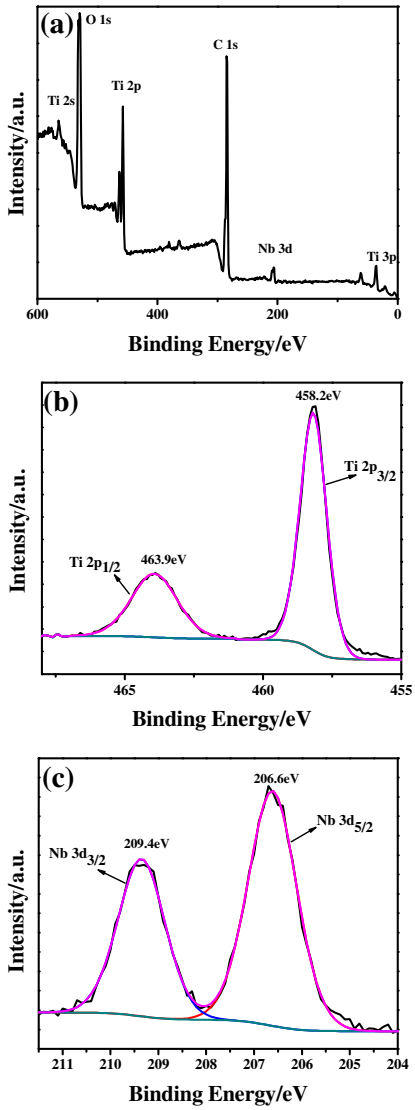

Fig. 6: (a) Wide-survey XPS spectrum of 5% Nb-doped TiO_2; (b) Ti 2p XPS spectrum; (c) Nb 3d XPS spectrum.

The composition of the samples was further analysed by XPS. The presence of Nb, Ti, O, and C can be seen from the wide-survey XPS spectrum of 5% Nb-doped TiO_2 (Fig. 6a). The Nb content based upon XPS analysis is about 4.7%, very close to the expected value. The as-planned 1 % and 2 % Nb contents are found to be 0.3% and 1.7% (based upon XPS data), respectively. We note that quantification based upon XPS survey spectra is known to have errors.

The corresponding narrow-scan XPS spectrum of Ti 2p for the 5% Nb doped TiO_2 shows that it consists of two peaks at around 458.2 eV (Ti $2p_{3/2}$) and 463.9 eV (Ti $2p_{1/2}$) (Fig. 6b). The positions and shapes of the XPS peaks indicate that the titanium is present as Ti^{4+} ions in the Nb-doped TiO_2. The peaks for Nb $3d_{5/2}$ and Nb $3d_{3/2}$ electrons are located at 206.6 eV and 209.4 eV for the 5% Nb-doped sample (Fig. 6c), which confirms the Nb^{5+} oxidation state. It is well known that Nb doping increases the electronic conductivity,[24, 29, 30] which would be

conducive to the electrochemical performance of the TiO_2 anode in this study.

Overall, Nb-doped TiO_2 shows better electrochemical performance than the pristine anatase, with the 2% Nb-doped electrode showing the best performance at 0.1 C at room temperature (Fig. 7a). The 1%, 2%, and 5% Nb-doped TiO_2 delivers a reversible capacity of 157.5, 169, and 164.9 mAh/g at 0.1 C after 100 cycles, respectively, while the pristine TiO_2 retained a charge capacity of 144.5 mAh/g after 100 cycles. Apparently, doping with Nb has enhanced the capacity of the TiO_2 electrode. The Nb-doped TiO_2 also exhibits excellent rate capacity (Fig. 7b), as the 2% Nb-doped TiO_2 delivers a capacity of 177.9 mAh/g at 0.1 C and 108.8 mAh/g at 5 C, while the pristine TiO_2 delivers 150.4 mAh/g at 0.1 C and only 54.6 mAh/g at 5 C.

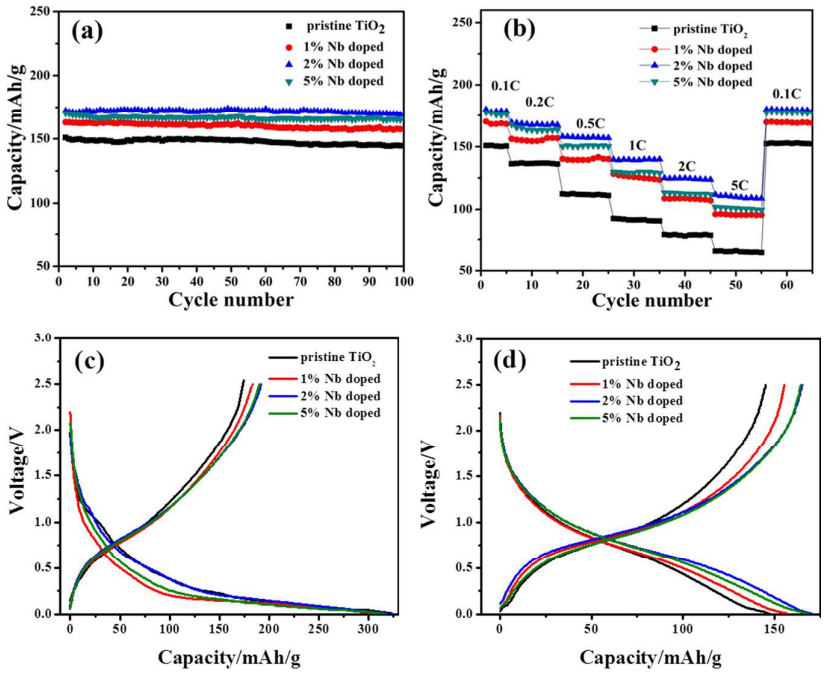

Fig. 7 (a) Cycling performance for the samples with different Nb doping levels at 0.1 C in the voltage range between 0-2.5 V; (b) rate performances of all samples at 0.1 C, 0.2 C, 0.5 C, 1 C, 2 C, 5 C, and 0.1 C; (c) initial charge and discharge curves at 0.1 C; (d) 100th cycle charge and discharge curves at 0.1 C.

Fig. 7c and 7d shows the initial and 100th cycle galvanostatic discharge/charge curves of the pristine and Nb-doped electrodes between 2.5 and 0 V at the rate of 0.1 C. The first discharge and charge capacity for the pristine TiO_2 is 323.8 mAh/g and 178.3 mAh/g, respectively, leading to an irreversible capacity of 145.5 mAh/g. With similar discharge capacities to that of pristine TiO_2, the 1%, 2%, and 5% Nb-doped TiO_2, however, show slightly lower irreversible capacities of 129.0, 132.8, and 127.7 mAh/g, respectively. The irreversible capacity in the first cycle may be due to the side reactions, such as the reactions with trace water adsorbed on the TiO_2 surface, and the decomposition of electrolyte and/or sodium ions intercalated into irreversible sites.[2, 15] Comparing the charge capacity at the 100th cycle (Fig. 7d) with that at the 1st cycle, it is clear that the Nb-doped samples also deliver better capacity retention compared with pristine TiO_2.

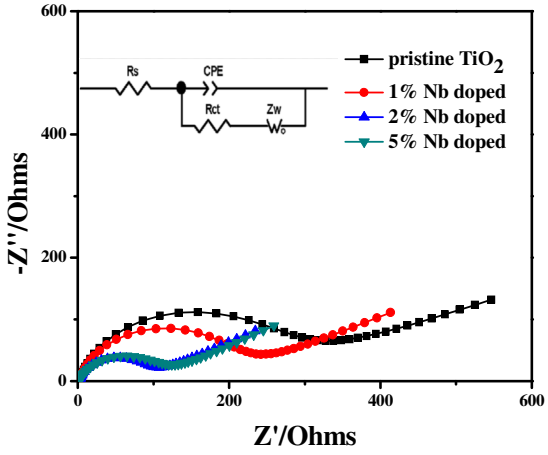

Fig. 8 Electrochemical impedance spectra of pristine and Nb-doped TiO_2 (inset: the equivalent circuit).

The Nyquist plots of all the samples were collected at a stable open circuit potential after a 6 h rest following discharge to 0.3

V, and the corresponding equivalent circuit (inset) shows that the semicircles for the doped samples are smaller than that for the pristine TiO_2 (Fig. 8). A more detailed analysis of the impedance spectra was undertaken on the basis of the proposed equivalent circuit, where R_s is the solution resistance, R_{ct} is the charge transfer resistance, and W is the Warburg impedance. CPE represents the constant phase angle element. The value of R_{ct} was obtained by applying Autolab software to simulate electrochemical impedance spectroscopy (EIS) data. The calculated impedance parameters are summarized in Table 1. All the samples show similar R_s, but the Nb-doped TiO_2 samples show much lower R_{ct} than that of the pristine TiO_2, indicating the effectively improved electronic conductivity of TiO_2 due to doping. The linear part of the EIS, which is directly related to long-range Na^+ diffusion in the bulk of the electrode, has been used to calculate the Na^+ diffusion coefficient by the following equation:

$$D = R^2T^2/2A^2n^4F^4C^2\sigma^2 \quad (1)$$

Where R is the gas constant 8.314 J/mol·K), T is the absolute temperature (298.15K), n is the number of electrons transferred per molecule during the reaction, F is the Faraday constant (96500 C/mol), A is the surface area of the electrode (1.54 cm^2), C is the concentration of Na ions(1.7×10^{-2} mol/cm^3), and σ is the Warburg factor, which can be obtained from the slope of the line $Z' - \omega^{-1/2}$ （shown in Table 1）. The calculated sodium diffusion coefficient D ($cm^2\ s^{-1}$) of the 2% Nb-doped material is 4.31×10^{-13} $cm^2\ s^{-1}$, 3.4 times higher than that of the pristine TiO_2 (1.29×10^{-13} $cm^2\ s^{-1}$), which indicates that the Nb-doping increases the Na^+ mobility of TiO_2. This enhancement is likely to be due to the expansion of the Na-ion migration channels by Nb-doping, as evidenced by the XRD and TEM analysis (Figs. 2, 4). Consequently, the rate performance of TiO_2 can be improved effectively, which is consistent with the charge-discharge results (Fig 7b). At 5 % doping, the performance, in terms of both capacity and rate capability, is slightly inferior to that of the 2 % sample, but still much better that that of the pristine TiO_2. The EIS analysis shows that higher doping levels would increase charge transfer resistance and lower the sodium diffusion coefficient.

Table 1: Solution resistance (R_s) and charge transfer resistance (R_{ct}) derived from the equivalent circuit model, the Warburg factor (σ), and the Na^+ diffusion coefficient (D_{Na+}) of pristine and Nb-doped TiO_2.

sample	Pristine TiO_2	1% Nb-doped	2% Nb-doped	5% Nb-doped
R_s (Ohms)	2.07	2.01	1.95	2.22
R_{ct} (Ohms)	223	188	82.2	115
σ	167.4	130.7	91.2	99.3
D ($10^{-13}cm^2/s$)	1.29	2.10	4.31	3.67

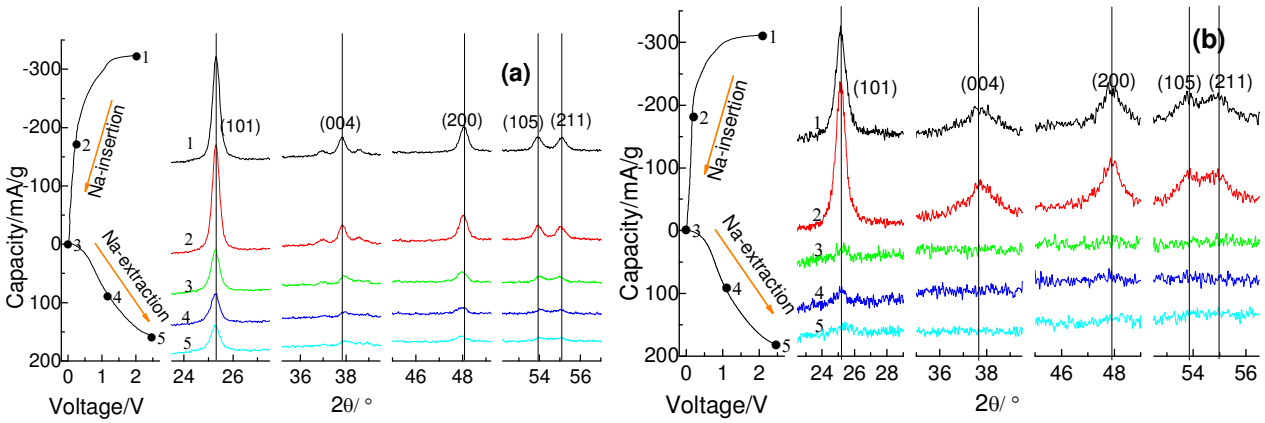

Fig. 9 Ex-situ XRD patterns of the pristine TiO_2 (a) and the 2% Nb doped TiO_2 (b) at various states of charge (SOCs) during the first discharge-charge process.

The mechanism of reversible sodium storage in anatase TiO_2 has been studied in previous reports. Kim et al.[17] claim that the crystal structure of anatase TiO_2 remains unchanged and that the sodium ions could reversly (de-)insert into the lattice. The in-situ XRD results reported by Wu et al.[31] show, however, that the XRD reflection almost disappears in the fully discharged state and does not reappear in the following charge process. Both of them found, however, that the (200) and (101) reflections shifted to lower 2-theta angles after sodiation. To elucidate the effects of Nb-doping on the structural change in TiO_2 during Na^+ (de-)insertion, ex-situ XRD was carried out on pristine and 2% Nb doped TiO_2 at different states of charge (SOCs) during the first charge-discharge process (Fig. 9). During the discharge process, no obvious changes in the XRD patterns

were observed when the discharge cut-off voltage was 0.2 V. (The discharge specific capacity was about 135 mAh/g.) Since this is the first cycle discharge, it is likely that up to this point, the capacity predominately comes from surface reactions with little contribution from Na insertion. When discharged to 0 V (~320 mAh/g discharge capacity), the XRD peaks of pristine anatase TiO_2 become much weaker, while only the (101) reflection can be vaguely observed for the 2% Nb doped TiO_2. During the sodiation process, the (200) and (101) reflection peaks shift slightly to lower angles, while the (004) and (105) peaks shift to higher angles. This indicates expansion of the anatase lattice along the *a* direction and shrinkage along the *c* direction. The decreases in peak intensity indicate that both pristine anatase TiO_2 and Nb doped TiO_2 become mostly disordered during sodiation, and the crystallinity cannot be recovered upon Na^+ de-sodiation. This is in agreement with the in-situ XRD result reported by Wu et al.[31]. Usui et al.[14] reported that the diffraction peaks of rutile TiO_2 shifted toward lower angle and the diffraction intensities weakened significantly during the sodiation process, while both the peak positions and the intensities can be recovered after desodiation. The difference in crystal structure between rutile and anatase TiO_2 could lead to different diffusion paths and accommodation sites, as predicted by DFT simulations[20], which could, in turn, cause different phase changes during sodiation and desodiation. Nb-doping seems to not be beneficial for maintaining the crystal structure, even though it can enlarge the lattice parameter of anatase TiO_2. The (101) reflection can still be observed in both the pure and doped anatase TiO_2, suggests that maybe the structure of TiO_2 is short-range ordered. Therefore, the enlargement of the crystal lattice caused by Nb doping would still benefit Na^+ ion migration.

Conclusions

Pristine and Nb-doped anatase TiO_2 particles were successfully synthesized via a sol-gel method. The TiO_2 sample with 2% Nb doping shows better rate capability and cycling stability. The 2% Nb-doped TiO_2 delivered a capacity of 177.9 mAh/g at 0.1 C and 108.8 mAh/g at 5 C, in contrast to 150.4 mAh/g at 0.1 C and only 54.6 mAh/g at 5 C for pristine TiO_2. The excellent rate capability can be attributed to the Nb doping, which increases the electronic conductivity and the Na^+ diffusion rate through enlarging the migration channels. This finding indicates that the Nb-doped TiO_2 materials can be attractive candidate anode materials for sodium ion batteries.

Acknowledgments

This work was supported by the Science and Technology Commission of Shanghai Municipality (No: 14DZ2261000). The access to facilities at the Institute for Superconducting and Electronic Materials at UOW is greatly appreciated. The authors would like to thank Dr. Tania Silver for polishing the manuscript, and ISEM and the Electron Microscopy Centre (EMC) for their support.

Notes and references

1. G. Xu, B. Ding, J. Pan, P. Nie, L. Shen and X. Zhang, *Journal of Materials Chemistry A*, 2014, **2**, 12662-12676.
2. Z. Bi, M. P. Paranthaman, P. A. Menchhofer, R. R. Dehoff, C. A. Bridges, M. Chi, B. Guo, X.-G. Sun and S. Dai, *Journal of Power Sources*, 2013, **222**, 461-466.
3. B. Dunn, H. Kamath and J.-M. Tarascon, *Science*, 2011, **334**, 928-935.
4. Y. Hu and X. Sun, *Journal of Materials Chemistry A*, 2014, **2**, 10712-10738.
5. J. M. Tarascon and M. Armand, *Nature* 2001, **414**, 359-367.
6. J. M. Tarascon, *Philos. Trans. R. Soc*, 2010, **368**, 3227-3241.
7. D. A. Stevens and J. R. Dahn, *J. Electrochem. Soc.*, 2000, **147**, 1271-1273.
8. S. Wenzel, T. J. Hara, J. and P. Adelhelm, *Energy Environ. Sci.*, 2011, **4**, 3342-3345.
9. L. Wu, D. Buchholz, D. Bresser, L. Gomes Chagas and S. Passerini, *Journal of Power Sources*, 2014, **251**, 379-385.
10. H. Xiong, M. D. Slater, M. Balasubramanian, C. S. Johnson and T. Rajh, *The Journal of Physical Chemistry Letters*, 2011, **2**, 2560-2565.
11. B. Guo, K. Yu, H. Fu, Q. Hua, R. Qi, H. Li, H. Song, S. Guo and Z. Zhu, *Journal of Materials Chemistry A*, 2015, **3**, 6392-6401.
12. G. Qin, X. Zhang and C. Wang, *Journal of Materials Chemistry A*, 2014, **2**, 12449-12458.
13. J. C. Perez-Flores, C. Baehtz, A. Kuhn and F. Garcia-Alvarado, *Journal of Materials Chemistry A*, 2014, **2**, 1825-1833.
14. H. Usui, S. Yoshioka, K. Wasada, M. Shimizu and H. Sakaguchi, *ACS Applied Materials & Interfaces*, 2015, **7**, 6567-6573.
15. F. Li, L. L. Yang, G. Xu, X. Q. Huang, X. Yang, X. Wei, Z. H. Ren, G. Shen and G. R. Han, *Journal of Alloys Compounds*, 2013, **577**, 663-668.
16. Y. Xu, E. M. Lotfabad, H. Wang, B. Farbod, Z. Xu, A. Kohandehghan and D. Mitlin, *Chemical Communications*, 2013, **49**, 8973-8975.
17. K. T. Kim, G. Ali, K. Y. Chung, C. S. Yoon, H. Yashiro, Y. K. Sun, J. Lu, K. Amine and S. T. Myung, *Nano Lett*, 2014, **14**, 416-422.
18. S. M. Oh, J. Y. Hwang, C. S. Yoon, J. Lu, K. Amine, I. Belharouak and Y. K. Sun, *ACS Applied Materials & Interfaces*, 2014, **6**, 11295-11301.
19. X. Yan, Y. Q. Zhang, K. Zhu, Y. Gao, D. Zhang, G. Chen, C. Z. Wang and Y. J. Wei, *Journal of Power Sources*, 2014, **246**, 95-102
20. D. Su, S. Dou and G. Wang, *Chemistry of Materials*, 2015, DOI: 10.1021/acs.chemmater.5b02348, 150818142825005.
21. K. Zhu, X. Liu, J. Du, J. Tian, Y. Wang, S. Liu and Z. Shan, *Journal of Materials Chemistry A*, 2015, **3**, 6455-6463.
22. P. S. Archana, R. Jose, T. M. Jin, C. Vijila, M. M. Yusoff and S. Ramakrishna, *Journal of the American Ceramic Society*, 2010, **93**, 4096-4102.
23. M. Fehse, S. Cavaliere, P. E. Lippens, I. Savych, A. Iadecola, L. Monconduit, D. J. Jones, J. Rozière, F. Fischer, C. Tessier and L. Stievano, *The Journal of Physical Chemistry C*, 2013, **117**, 13827-13835.
24. Y. Wang, B. M. Smarsly and I. Djerdj, *Chemistry of*

Materials, 2010, **22**, 6624-6631.
25. Y. Liu, J. M. Szeifert, J. M. Feckl, B. Mandlmeier, J. Rathousky, O. Hayden, D. Fattakhova-Rohlfing and T. Bein, *ACS Nano*, 2010, **4**, 5373-5381.
26. Y. Furubayashi, T. Hitosugi, Y. Yamamoto, K. Inaba, G. Kinoda, Y. Hirose, T. Shimada and T. Hasegawa, *Appl Phys Lett*, 2005, **86**,252101.
27. X. Lü, X. Mou, J. Wu, D. Zhang, L. Zhang, F. Huang, F. Xu and S. Huang, *Advanced Functional Materials*, 2010, **20**, 509-515.
28. A. K. Chandiran, r. F. d. Sauvage, M. Casas-Cabanas, P. Comte, S. M. Zakeeruddin and M. Graetzel, *The Journal of Physical Chemistry C*, 2010, **114**, 15849-15856.
29. A. M. Ruiz, G. Dezanneau, J. Arbiol, A. Cornet and J. R. Morante, *Chemistry of Materials*, 2004, **16**, 862-871.
30. A. V. Manole, M. Dobromir, M. Gîrtan, R. Mallet, G. Rusu and D. Luca, *Ceramics International*, 2013, **39**, 4771-4776.
31. L. Wu, D. Bresser, D. Buchholz, G. A. Giffin, C. R. Castro, A. Ochel and S. Passerini, *Advanced Energy Materials*, 2015, **5**, 1401142.

Journal Name

ARTICLE

Table of Content

Niobium doped anatase TiO_2 as an effective anode material for sodium-ion batteries

Fei Zhao[a], Baofeng Wang[a,b,*], Yufeng Tang[c], Zhenguo Huang[b,*], Honghua Ge[a] ,Hua Kun Liu[b]

Nb-doped anatase TiO_2 anode materials with high reversible sodium storage capacities, excellent cycling stability and rate capability were synthesized by sol-gel method.